ENGINEERING Environment
2026, 20(4): 64 https://doi.org/10.1007/s11783-026-2164-2

RESEARCH ARTICLE

Emission of fine and ultrafine nanoparticle aerosols from composites functionalized with Multi-Wall Carbon Nano Tubes (MWCNTs) subjected to sliding wear: the influence of matrix material

Francisca Husanu[1], Juan Camilo Vélez Molina[1,2], Jesús Antonio Carlos Cornelio[1], Juan Felipe Santa Marín[1], Alejandro Toro[2], Marta Castellote[1], Roman Nevshupa ✉ [1]

1. Spanish National Research Council, Eduardo Torroja Institute of Construction Science (IETCC-CSIC), Madrid 28033, Spain
2. Universidad Nacional de Colombia, Medellin 050034, Colombia

HIGHLIGHTS

- MWCNTs-cement composite has higher aerosol emissivity than porous neat cement paste.
- Liberation of MWCNTs from cement and polymer matrixes is negligibly low.
- MWCNTs influence aerosol emission indirectly by alteration composite properties.
- The effect of MWCNTs on emissivity was associated with the wear mechanism.

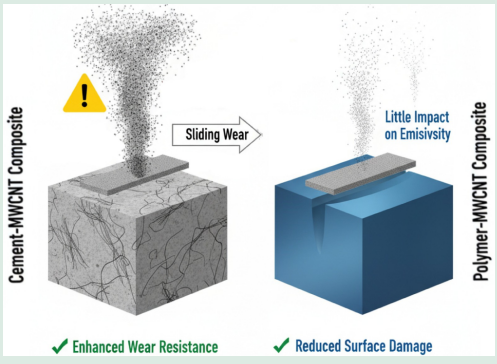

ABSTRACT: While multi-wall carbon nanotube (MWCNT)-reinforced nanocomposites offer improved wear resistance, the health implications of released nanoparticle aerosols are a concern. This research aimed to understand the influence of matrix material on the tribological properties, microstructure, and triboemission of MWCNT-functionalized polymer and cement composites. Key findings reveal that aerosol emission cannot be predicted solely based on porosity and mechanical properties. The observed variations in MWCNT effects across different matrix materials are attributed to the distinct dominant wear mechanisms in each.

KEYWORDS: Composite, Triboemission, MWCNT, Nanoparticles, Cement, Vinyl ester

1 Introduction

Multi-wall carbon nanotubes (MWCNTs) are widely recognized for their high mechanical strength, large aspect ratio, and excellent electron mobility, making them ideal for reinforcing and functionalizing composite materials with polymeric, ceramic, metallic, and cementitious matrices (Zhang et al., 2006; Campo et al., 2015; Sedaghatdoost and Behfarnia, 2018; Chen and Akono, 2020; Cerro-Prada et al., 2021; Feijoo et al., 2021). These nanocomposites offer the advantage of producing materials that are simultaneously stronger, lighter, and more resistant to wear and tear.

However, as with other engineered nanomaterials

✉ Corresponding author. E-mail: r.nevshupa@csic.es

Article history: Received 3 April 2025, Revised 16 October 2025, Accepted 14 December 2025, Available online 30 January 2026

(ENMs), realistic scenarios exist in which carbon nanotubes may be released from nanocomposites due to mechanical damage, potentially leading to unintended human or environmental toxicity. Such scenarios include machining processes—such as drilling or sawing—during manufacturing, abrasion during regular service life, and crushing at the end-of-life stage.

In view of the complexity and interdisciplinary nature of this issue, various approaches have been employed to investigate it (Fig. S3) (refer to Electronic Supplementary Material). A substantial body of research has focused on quantifying exposure to nanoscale particles and fibres in workplace environments, using both simulated experiments and direct on-site measurements (Thompson et al., 2015; Boonruksa et al., 2016; Debia et al., 2016; Guseva Canu et al., 2016; Sharma et al., 2016). The toxicity of dust generated from mechanical abrasion of MWCNT nanocomposites has been evaluated using *in vitro* models, as well as studies on rodents and humans (Borm et al., 2006; Wohlleben et al., 2013; Saber et al., 2015; Christou et al., 2016; Schraufnagel, 2020).

Given the critical importance of aerosol characteristics for both exposure and toxicity assessments, most studies have carefully measured particle size distribution (PSD), particle number concentration (PNC), and particle mass concentration (PMC) using direct-reading instruments. Morphological and chemical properties of aerosol particles have also been extensively analysed using filter-based sampling, electrostatic precipitators, and other collection devices. However, only a few studies have successfully determined kinetic parameters of aerosol emission—such as total and specific emission rates—which require advanced techniques like isotope labelling (Hennig et al., 2019; Zhao et al., 2023) or solving mass balance equations (Koivisto et al., 2012; Gomez et al., 2014; Heitbrink and Lo, 2015; Morgeneyer et al., 2015). Recently, significant improvements to the latter method have enabled accurate quantification of both the rate and absolute number of released particles without the need for complementary tests (Nevshupa et al., 2020).

In parallel, a large volume of material-oriented studies has explored how aerosol emissions depend on the type of matrix, filler content, and mechanical action. Researchers have noted that nanofillers exert a complex and often non-linear influence on nanoparticle emission (Shandilya et al., 2014). In his comprehensive review Duncan (Duncan, 2015) highlighted conflicting findings, even for identical filler/host combinations. For example, Huang et al. (2012) observed a clear positive correlation between CNT concentration in epoxy and the number concentration of released particles, whereas Bello et al. (2009) and Wohlleben et al. (2011) found no significant differences between nanocomposites and their reference materials.

Matrix polymer properties (Kang et al., 2017) and the intensity of mechanical stress (Golanski et al., 2011, 2012) are also important factors controlling aerosol emissions during sanding of polymer-matrix composites containing CNTs. While no measurable aerosol emission was found using a standard Taber abrasion test or cutting with a band saw, under more realistic mechanical stress conditions such as abrasion, scratching, and mechanical shocks notable emission occurred (Heitbrink and Lo, 2015).

Systematic investigations have linked MWCNT release to high filler content (30%) and/or the presence of CNT agglomerates acting as predefined failure points (Golanski et al., 2012; Wohlleben et al., 2013). Free CNTs were occasionally observed under conditions of severe abrasion. Numerous studies using industry-relevant processes—including crushing (Ogura et al., 2017), grinding (Ogura et al., 2013, 2015; Boonruksa et al., 2016; Kovochich et al., 2018; Zhao et al., 2023), drilling (Bello et al., 2010; Ding et al., 2017; Starost et al., 2017), sanding (Gupta et al., 2006; Cena and Peters, 2011; Huang et al., 2012; Hirth et al., 2013; Wohlleben et al., 2013; Gomez et al., 2014; Heitbrink and Lo, 2015; Saber et al., 2015; Kang et al., 2017), cutting (Ogura et al., 2019), scratching and abrasion (Gupta et al., 2006; Golanski et al., 2012), sawing (Methner et al., 2012; Gomez et al., 2014; Heitbrink and Lo, 2015; Ding et al., 2017; Starost et al., 2017; Ogura et al., 2019; Hedmer et al., 2022), ball milling (Jiang et al., 2014), high-energy tensile rupture tests (Schlagenhauf et al., 2015), tension fatigue (Ren et al., 2003), and low-energy manipulation (e.g., tapping, shaking, wiping, and handling) (Methner et al., 2012; Hennig et al., 2019)—support the conclusion that mechanical forces alone do not typically result in the release of free CNTs. Such release was only clearly observed after degradation of the polymer matrix and the application of very high shear forces.

Several studies have also examined aerosol generation and ENM release from cement-based composites containing carbon nanotubes using Taber abrasion to simulate normal wear (Wohlleben et al., 2011, 2024) and high-energy sanding (Hirth et al., 2013). Comparisons between nanocomposites and reference materials without nanofillers revealed insignificant differences in both particle number concentrations and aerosol size distributions during normal use (Wohlleben et al., 2011). Chemical analysis and SEM observations of worn surfaces did not indicate CNT release, although a few CNTs were found dangling

from cement debris in sanding powder.

The experimental findings suggest that nanoparticle aerosol triboemission is influenced by both the host material and the nanofillers which determine the composite's mechanical properties—such as strength, hardness, wear resistance, and fracture toughness (Schlagenhauf et al., 2012; Shandilya et al., 2015). Nanofillers can indirectly affect aerosol emissions by altering mechanical properties, porosity, and other structural characteristics. For example, adding 0.1 wt.%–0.5 wt.% MWCNTs to a cement matrix significantly enhances the formation of high-density calcium silicate hydrates, the primary binder phase in Portland cement. This results in reduced porosity and a 9.4%–14.0% increase in fracture toughness (Makar and Chan, 2009; Chen and Akono, 2020), which are expected to lower aerosol emissions. This is because the collapse and fragmentation of porous structures are key mechanisms of aerosol generation. Lower porosity and higher strength reduce structural degradation during abrasion, thereby decreasing emission rates. Interestingly, while nanofillers can increase mechanical strength in inorganic matrices, they may also increase porosity, potentially compromising structural integrity and enhancing aerosol generation. In wood, however, higher porosity has been shown to reduce triboemission of aerosols (Shandilya et al., 2015; Piscitello et al., 2021). Apart from improving mechanical strength, the incorporation of MWCNTs into organic matrices improves thermal stability and wear resistance (Zhang et al., 2009; Wu et al., 2021; Rahman et al., 2022), while also reducing friction (Kim et al., 2022). These factors are expected to decrease the aerosol emission.

It should also be noted that MWCNTs and other nanofillers are susceptible to tribochemical transformations. These nanomaterials can participate in tribochemical reactions at contact surfaces, resulting in the generation of nanoparticles with chemical compositions distinct from both the matrix and the additives. Recent studies have shown that MWCNTs—like other carbonaceous materials—are prone to amorphization under abrasion (Ye et al., 2019; Shirasu et al., 2020). In the presence of oxygen, water vapour, and sulfur, mechanical stress of carbonaceous phases can lead to the tribochemical synthesis of methane, carbon monoxide and dioxide, carbonyl compounds, hydrogen sulfide, and carbon disulfide (Rusanov et al., 2015a, 2015b; Cornelio et al., 2016; Igartua et al., 2017; Vélez et al., 2020; Muñoz-Cortés et al., 2024). The synergism and tribochemical affinity between carbon and siloxane groups has also been well documented (Xie et al., 2021).

To disentangle these complex relationships, a quantitative study of nanoparticle aerosol emissions from composite materials is urgently needed. This study employs a novel method to comparatively assess fine and ultrafine particle emissions from two composite materials: a cement-paste matrix and a vinyl-ester-resin matrix, both functionalized with MWCNTs. The cement paste serves as a simplified model for concrete reinforced with MWCNTs, a promising material for road pavement applications (Ezzat et al., 2023). Meanwhile, MWCNT-reinforced polymer composites are designed for use as top-of-rail friction modifiers to regulate friction and wear at wheel–rail interfaces (Vélez et al., 2020).

The study specifically focuses on fine and ultrafine fractions, which—despite contributing minimally to total aerosol mass—are highly relevant due to their abundance and small size, posing significant implications for respiratory health and climate impact. The emissivity parameter was used as an effective tool to quantify the number of fine and ultrafine particles—across different size ranges—generated from a unit volume of crushed material, thereby providing insight into the material's intrinsic capacity to produce these aerosol fractions.

2 Materials and methods

2.1 Materials

The MWCNTs were synthesized via chemical vapor deposition using acetylene as a precursor. The reaction was conducted at 700 ºC in a high-precision furnace equipped with a quartz tube. Acetylene was used as a carbon source. The process gas was composed from nitrogen, acetylene and hydrogen at the ratios 80:20:15. The total gas flux was 115 cm^3/min. Nickel catalyst was employed. The process involved a catalyst reduction phase of 20 min, a MWCNT growing phase of 30 min, and a cooling phase of 60 min. The structure of obtained MWCNTs is shown in Figure S4. The MWCNT diameter ranged from 12 to 35 nm, while their length was between 10 and 20 μm (Hoyos-Palacio et al., 2019; Cornelio et al., 2022).

The cement paste was prepared using CEM I 52.5 R Portland cement, water (with a water-to-cement ratio of 0.39), and a superplasticizer (SIKAPLAST®-1003, 1 wt.% relative to the water content). The MWCNTs were dispersed in the water/superplasticizer solution using a high-speed stirrer for 30 min. This method was selected due to the large batch volume and to prevent damage or shortening of the MWCNTs that can occur during sonication (Rennhofer and Zanghellini, 2021).

Previous studies have shown that superplasticizers enhance MWCNTs dispersion (Kim et al., 2024). The suspension of MWCNTs were added to cement and mixed according to UNE-EN196-1 standard. The paste was cast into rectangular dies (5 cm × 5 cm × 3 cm) and cured for 28 days in a controlled environment, with a constant temperature of 21 °C and relative humidity of 95%. Reference samples (Cem_R) were prepared following the same procedure without addition of MWCNTs. The composite samples are denoted Cem. Electron micrographs of pristine and worn surfaces of cured samples did not reveal significant clumping of MWCNTs (refer to Figs. 7 and 8).

To prepare polymer-matrix composites vinyl ester resin 805 (Protokimica S.A.) was mixed with MWCNTs using a high-speed mixer followed by sonication. The mixture was heated under controlled conditions, and a catalyst was gradually added, maintaining an 8:100 catalyst-to-resin weight ratio. The mixture was cast into cylindrical molds, 13 mm in diameter, and cured at 80 °C for 24 h. Reference samples ($Poly_R$) were prepared following the same procedure without addition of MWCNTs. The composite samples are denoted Poly.

2.2 Characterization methods

An original experimental system designed to accurately quantify the rates of aerosol triboemission was used. The system is based on a pin-on-disk tribometer (Fig. S6) equipped with an aerosol-tight chamber, 14.6 L in volume. Cementitious specimens were placed on a turntable and abraded using a static, 20 mm in diameter alumina ceramic ball.

To simulate the sliding conditions of a top-of-rail friction modifier, which is usually pressed against a moving wheel, an inverse configuration was employed, where a stationary composite specimen was pressed against a rotating steel disk (tempered AISI 4340, hardness ~400 HV). Rectangular sheets of polymer composite or reference polymer were glued to a stationary pin holder. The normal load was 2.94 N. In the experiment with cement materials, the sliding velocity was 1 m/s. In the experiments with polymer materials, sliding velocity was 3.0 to 3.5 m/s. Number concentrations over a range of particle mobility diameter, D_p, of 10 to 400 nm were measured using a Scanning Mobility Particle Sizer (SMPS) (Model DMA 3910, TSI Inc.). The flow rate was 0.75 L/min and the sampling interval was 1 min. A 70-mm stainless-steel pipe linked the aerosol generation chamber to the SMPS, maintaining a uniform distance between the tribometer and the pipe's inlet. The accuracy of size distribution measurements is estimated to be within ±15%, while the repeatability of particle counting carries an uncertainty of approximately 0.3%.

The experimental procedure consisted of the following steps:

(1) Establishing steady background aerosol concentrations at a very low level (typically below 30 #/cm^3 in the whole range 10–400 nm) using HEPA EU14 filters of the aerosol booth.

(2) Abrading the samples for 15 min (unless otherwise stated).

(3) Measuring aerosol concentrations before and during abrasion.

(4) Measuring aerosol concentration decay after the end of the test until the concentration returns to the background value.

(5) Repeating the experiment using an aerosol sampler to capture airborne nanoparticles following the sampling method outlined by R'Mili et al. (2013).

The emission rate for each particle size range was calculated using the following expression (Nevshupa et al., 2020):

$$K_{te,i}(t)=V\left(\frac{dC_i}{dt}+\frac{C_i(t)}{\tau_i}\right)-Q_0C_{0,i}, \quad (1)$$

where τ_i is the time constant of the exponential decay of aerosol concentration (i-th size range), $C_i(t)$ is the instant aerosol concentration, $C_{0,i}(t)$ is the background aerosol concentration in the aerosol booth, Q_0 is the rate of the air sampling and V is the volume of the aerosol-tight chamber.

Figure S5 (refer to Electronic Supplementary Material) depicts a typical time series of aerosol concentration in the particle size range D_p 116 nm showing the increase during abrasion and a transient decay after the end of the test. The transient decay was fitted using an exponential function yielding the τ_{116}.

For the constant volume of aerosol-tight chamber and aerosol sampling conditions the time constant is inversely proportional to the effective aerosol deposition velocity. Bearing in mind that diffusion is the rate-controlling step for fine and ultrafine aerosol deposition, variation of the diffusion rate due to the changes in the particles' density or shape can be traced by the analysis of the time constant $\tau_{2,i}$ (Scheuch and Heyder, 1990; Wahlström et al., 2010; Kulkarni et al., 2011; Chen et al., 2017; Nosko et al., 2017).

The volumetric wear of the cementitious specimens was measured using white-light confocal microscopy. The surface geometry of the mechanically affected zone was measured at twelve different positions along each circular wear track. The mean worn volume was determined by multiplying the mean cross-sectional

area by the circumference of the corresponding wear track.

For polymer composites, the total pore volume was determined using helium pycnometry. For cementitious materials, which exhibit more developed porosity than polymers, a Dynamic Vapor Sorption (DVS) system and mercury intrusion porosimetry were employed to determine the pore structure. The DVS system was calibrated using microcrystalline cellulose (20–300 μm) according to ASTM E2551. DVS tests were conducted at 25 °C, with relative humidity (RH) incrementally increasing from 3% to 90% in 10 steps. Subsequently, RH was decreased back to 3% in 9 steps. Each step included a three-hour stabilization period to ensure mass equilibrium.

Raman spectroscopic analysis with excitation laser wavelength of 780 nm was conducted on both worn and neighbouring pristine surfaces. Scanning electron microscopy (SEM) was employed to analyse the surface morphology of the samples and the captured airborne aerosol nanoparticles.

3 Experimental results and discussion

3.1 Kinetics and dynamics of aerosol emission

3.1.1 Relaxation time constants

Figure 1 presents the relaxation time constants (or residence times) obtained for various particle sizes. In the reference cement paste (Fig. 1(a)), the plot is nearly flat, with τ_i values ranging from 3 to 4 min. These values are approximately 50% lower than those reported for cement mortar (Husanu et al., 2024) and are similar to the time constants of smoke particles (Nevshupa et al., 2020). These low τ_i values suggest high mobility of the aerosol particles. Following the addition of MWCNTs, τ_i increased slightly within the 30–80 nm range, while remaining unchanged for other particle sizes. This behaviour is consistent with the findings of Husanu et al. (2024) for mortar blocks reinforced with polyurethane fibres.

3.1.2 The influence of particles' shape and density on relaxation time

The variations in τ_i following addition of MWCNTs can be attributed to the change in dynamic shape factor of aerosol particles due to a change in shape (increased irregularity or prolateness). The dynamic shape factor, as defined by Kasper (1982), is expressed as follows:

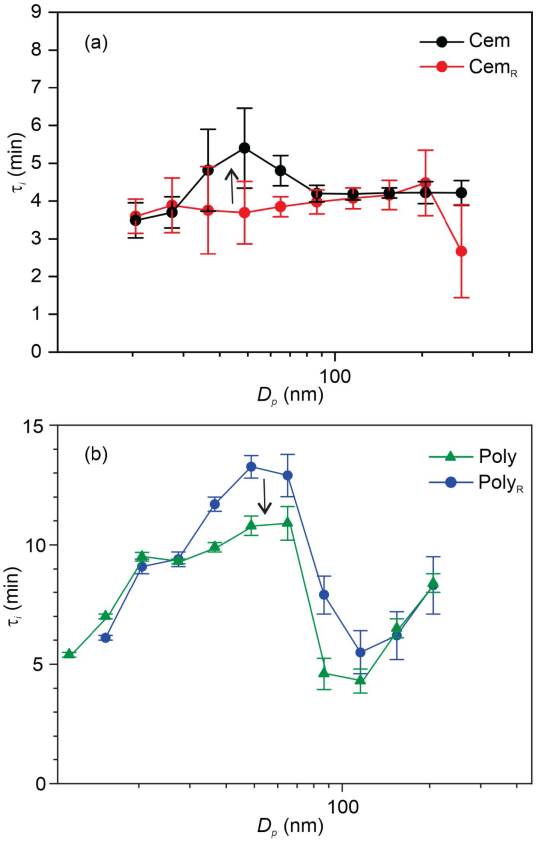

Fig. 1 The time constant of the transitional concentration decay as a function of particle mobility diameter for (a) cementitious matrix, (b) polymeric matrix.

$$k = \rho^{\frac{1}{3}} \left[\frac{D_p}{D_{ae}}\right]^{\frac{2}{3}} \frac{C_{ve}}{(C_{me}C_{ae})^{\frac{2}{3}}}, \quad (2)$$

where ρ is the bulk particle density, D_p is the electrical mobility particle diameter, D_{ae} is the equivalent aerodynamic particle diameter, C_{ve} is the volume equivalent slip coefficient, C_{me} is the mobility equivalent slip coefficient and C_{ae} is the aerodynamic equivalent slip coefficient.

The Cunningham slip correction factor, C, is a function of the Knudsen number (Kn), defined as the ratio of the gas mean free path to the particle radius (Decarlo et al., 2004), and therefore depends on particle size. In the continuum regime (large D_p), $Kn \rightarrow 0$ and $C \rightarrow 1$. In the transition regime ($0.1 < Kn < 10$), $C > 1$ and increases with Kn. Although analytic determination of k is complex, expression (2) enables comparing the aerodynamic characteristics of particles with the same mobility diameter but different shapes (or densities). Consider two particles with equal densities but different aerodynamic diameters, particles with smaller D_{ae} will exhibit higher diffusivity and faster relaxation. Recall that D_{ae} represents the equivalent diameter describing a

particle's sedimentation characteristics in response to an applied force acting upon its mass (Kasper, 1982). Analysis of aerosol particle micrographs helps to understand the observed variations in aerosol residence times.

Figure 2 presents micrographs of aerosol particles produced by the abrasion of Cem_R and Cem, captured on an amorphous hollow carbon film. The particles exhibit polygonal morphologies characteristic of cementitious materials (Batsungnoen et al., 2020; Feijoo et al., 2021; Concha-Lozano et al., 2025). In contrast to the findings of Hirth et al. (2013), no protruding MWCNTs were observed. Particle sizes ranged from approximately 20 nm to several micrometers, with larger particles appearing as agglomerates (Figs. 2(b) and 2(d)).

Energy-dispersive spectroscopy (EDS) analysis confirmed the presence of key cement paste elements: Si, O, Ca, Fe, Al, Na, and K. A more detailed examination of the magnified images reveals subtle differences in particle morphology between the reference and MWCNT-containing composites. Aerosol particles from the reference cement paste appear as isotropic, irregular polytopes, whereas those from the MWCNT composite tend to form lamellar-like polygons. The polygon morphology likely results from the fracturing of larger polytope crystals observed on pristine surfaces (Fig. 7(c)), aligning with recent findings (Onthong et al., 2025). These morphological features may be associated with the lower diffusivity and higher residence time of Cem aerosol particles, as shown in Fig. 1. Measurements of skeletal densities (Table 1) did not reveal any significant variations attributable to the incorporation of less dense MWCNTs (Rasmussen et al., 2014). Therefore, any effect of particle density on residence time is expected to be negligible.

Additionally, micrometer- and submicrometer-sized fibrous particles (hundreds of nanometers in length) were observed (highlighted by the red circle in Fig. 2(a)). These structures resemble fragments found on worn surfaces (Fig. 8). They formed sparse

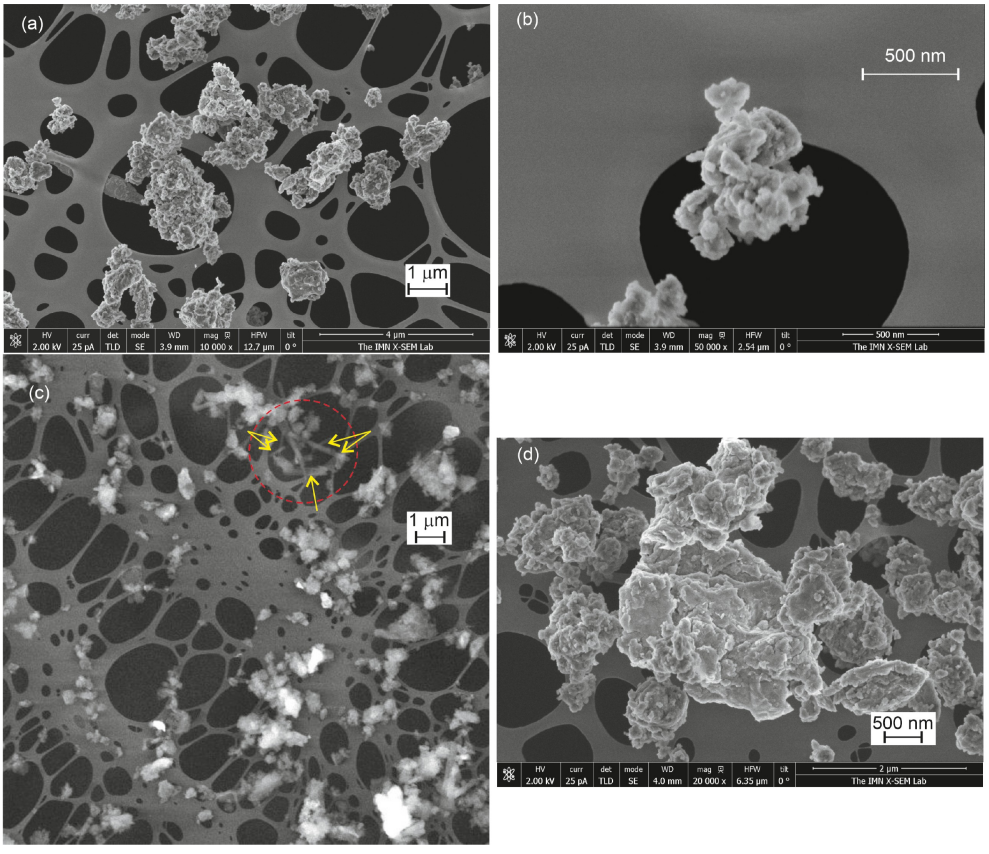

Fig. 2 Micrographs of aerosol particles produced by abrasion of Cem_R: (a) general view showing cement particles and (b) magnified view of cement particles and their agglomerates. Micrographs of aerosol particles produced by abrasion of Cem composite (c) general view showing cement particles and fibrous structures (marked by yellow arrows in the red circle), (d) magnified view of cement particles and their agglomerates. The particles are deposited on an amorphous hollow carbon film.

Table 1 Specific wear rate per sliding path and emissivity (mean ± standard error)

Parameter	Units	Sample			
		Cem_R	Cem	$Poly_R$	Poly
w_V	mm^3/m	$(1.58 \pm 0.113) \times 10^{-1}$	$(2.59 \pm 0.187) \times 10^{-2}$	$(8.04 \pm 0.683) \times 10^{-3}$	$(1.18 \pm 0.100) \times 10^{-2}$
Emissivity	$\#/mm^3$	$(0.268 \pm 0.019) \times 10^8$	$(3.97 \pm 0.287) \times 10^8$	$(5.37 \pm 0.46) \times 10^6$	$(5.52 \pm 0.47) \times 10^6$
Skeletal density	g/cm^3	–	–	1.11 ± 0.15	1.22 ± 0.14
Apparent density	g/cm^3	–	–	1.020 ± 0.005	1.040 ± 0.003
% of voids		–	–	8.82 ± 1.19	17.3 ± 1.99

agglomerates distinct from original MWCNT bundles. The geometric size range of these fibrous aerosol particles is notably larger than that of individual MWCNTs. Given their size, these structures are unlikely to be associated with the residence time variations shown in Fig. 1, as they fall outside the corresponding mobility diameter range. It is conceivable that these fibrous structures correspond to rod-like hydrated cement products, such as ettringite (Lu et al., 2020). Although such structures were rare, their potential health risks—particularly related to inhalation—warrant further investigation into their nature and origin.

Figure 3 presents micrographs of aerosol particles generated by abrasion of the reference polymer and its corresponding MWCNT-reinforced composite. Aerosol particles from the neat polymer exhibit thin polygonal or flake-like shapes normally ranged between 50 nm to 1 μm, consistent with previous reports (Schlagenhauf et al., 2012; Shandilya et al., 2014). The uniform contrast across each flake layer suggests their plane shape. The length and width range from EDS analysis confirmed the presence of only carbon and oxygen, and no protruding MWCNTs were observed. In contrast, aerosol particles from the composite exhibit more irregular featureless shapes. This morphology likely enhances their aerodynamic mobility and reduces residence time in contrast to neat polymer. This is consistent with the trend observed in Fig. 1. However, it remains unclear why this variation affected only a specific range of particle mobility diameters.

3.1.3 Kinetics and dynamics of aerosol emission

Figures 4(a), 4(c), 4(e), and 4(g) show the emission rates of aerosol particles across different sizes for the four materials studied. These rates were calculated using Eq. (1) and the τ_i values shown in Fig. 1. While both the rate and dynamics of aerosol emissions depended significantly on the matrix type, MWCNTs had only a minor influence on these parameters. The emission rate for cementitious materials was more than two orders of magnitude higher than that for the polymer materials. Figures 4(b), 4(d), 4(f), and 4(h) show the total emission rate within the size ranges indicated by the corresponding boxes in Figs. 4(a), 4(c), 4(e), and 4(g). For all materials, emissions began simultaneously with abrasion. For neat cement paste, emissions decreased quickly with time and almost ceased before the end of abrasion. For the cement composite, emissions were steadier during abrasion and ceased only afterward. It should be noted that the emission rate decreased with decreasing sliding speed for both composites. In the case of the polymer-matrix composite, no measurable emission was observed at speeds below 3 m/s.

The particle size range with the highest emission rate expanded slightly after the addition of MWCNTs, from 87–154 nm to 87–205 nm. Figure 5 shows the normalized distributions of aerosol particles by mobility diameter at times V_1, V_2, and V_3 for Cem and Cem_R. The data were fitted with lognormal functions. All distributions were bimodal, with a minor mode centred at 28 nm. The dominant mode (comprising approximately 98.4% of the total distribution) was centred at 126 nm for Cem_R and 163 nm for Cem. Taken together, these findings suggest that, for cement paste, MWCNT addition slightly decreased the emission rate in the 30–80 nm range while reducing particle diffusivity and increased the emission rate for particles with $D_p > 100$ nm.

For polymer materials, the emission dynamics were notably different. Emissions occurred as a series of events, beginning with larger particles (around 116 nm) and ending with smaller particles (below 60 nm). Each event lasted 3 to 5 min, with emission ceasing between events. The evolution of particle size during these events is clearly shown in Fig. 6, which presents normalized aerosol size distributions. The distributions for both $Poly_R$ and Poly were trimodal. The first mode, centred around 112–140 nm, dominated (98.6%) at the beginning of each emission event, decreasing to approximately 10% by the end. The second and third modes were centred at approximately 34–40 nm and

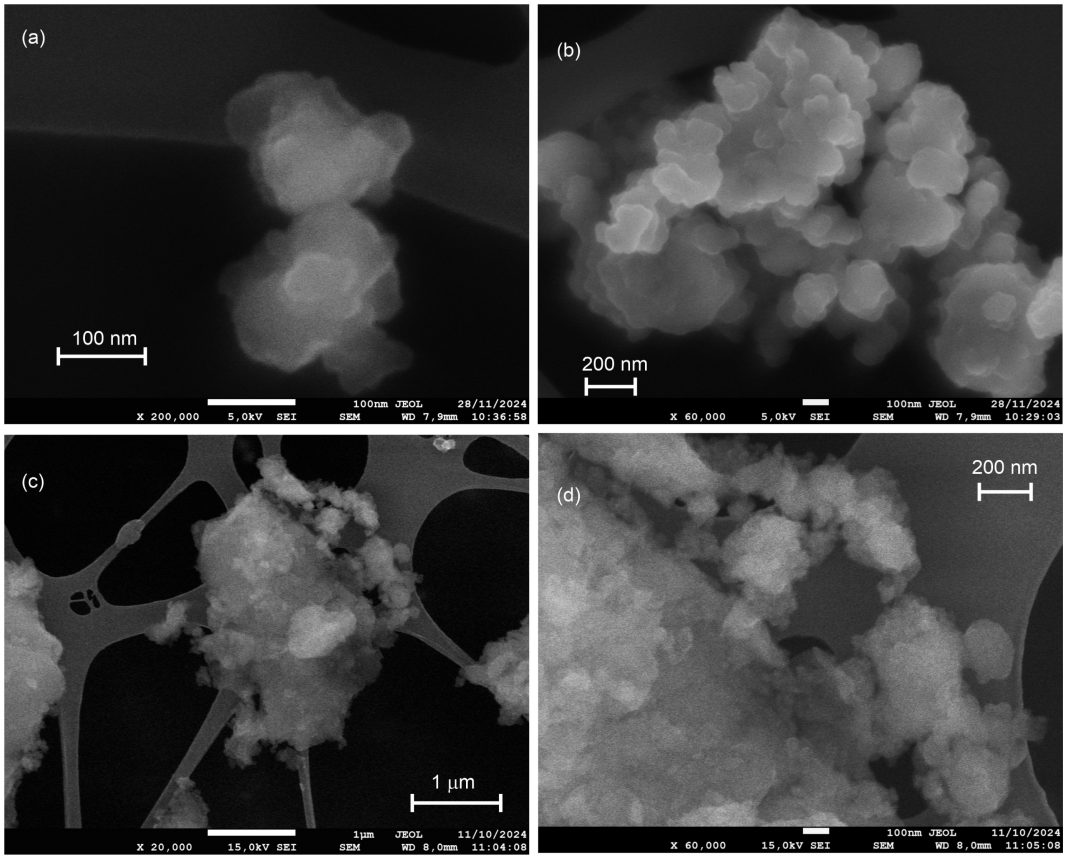

Fig. 3 SEM micrographs of aerosol particles produced by abrasion of $Poly_R$: (a) a small agglomerate, (b) a larger view. SEM micrographs of aerosol particles produced by abrasion of Poly: (c) ultrafine particles aggregated around a coarse particle, (d) a magnified view showing fine and ultrafine particles. The particles are deposited on an amorphous hollow carbon film.

16 nm, respectively. Similar to the cementitious materials, the mode around 30 nm remained unaffected by the addition of MWCNTs. As will be discussed in Section 3.3, unlike the cement samples, partial thermal oxidation in polymer aerosols cannot be entirely ruled out. The third mode observed in aerosols generated by polymer abrasion is consistent with thermal oxidation, as demonstrated in studies on the combustion of polymers and paper (Hammer et al., 2021). Furthermore, its contribution to total emissions increases over time as the polymer temperature gradually rises. However, to validate this hypothesis and clarify the mechanisms driving this aerosol mode formation, further chemical characterization of the emitted particles and gases is required.

3.2 Characterization of wear and determination of surface temperature

3.2.1 Specific wear rate

MWCNTs significantly improved the wear resistance of cement paste, resulting in a nearly six-fold decrease in the specific wear rate (Table 1). In contrast, the addition of MWCNTs increased the polymer wear rate by approximately 50%. This finding is consistent with previous works (Düzcükoğlu et al., 2015; Zhang et al., 2016), which also reported increased wear rates upon MWCNT addition. However, other researchers (Cui et al., 2013; Campo et al., 2015) found a significant decrease in wear rate with MWCNT addition in epoxy resin, especially at higher sliding velocities. It should be noted that the values presented in Table 1 represent apparent wear rates, determined under the assumption of linear wear behaviour. Notwithstanding, microscopic analysis (presented below) demonstrates that the polymer composite exhibits an intensive initial wear phase characterized by the formation of a transfer film on the counterpart, resulting in nonlinear wear behaviour. This suggests that the actual wear rate during the steady-state regime may be lower than the measured results.

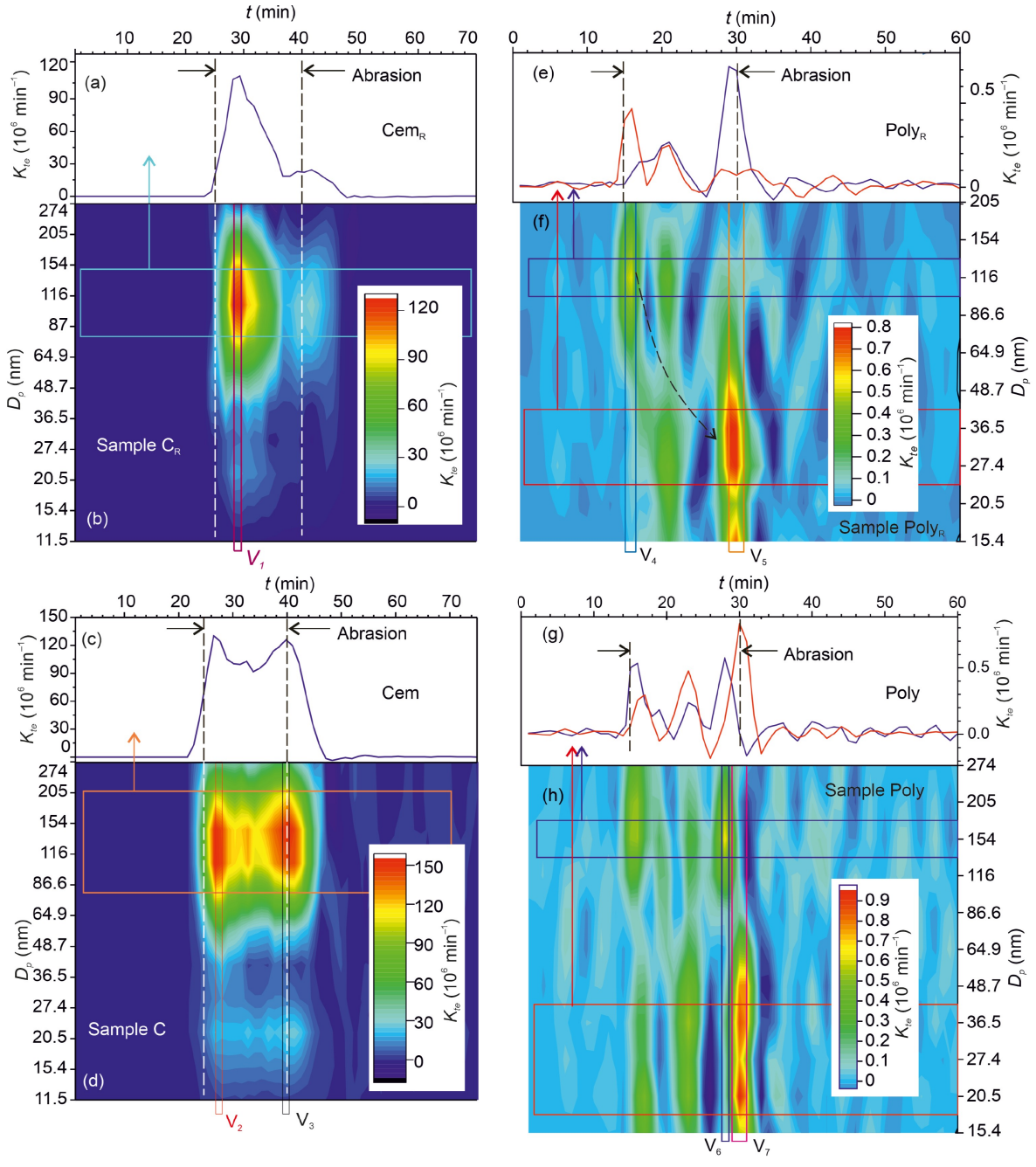

Fig. 4 Time series of emission rates as a function of particle size for samples: Cem_R (a), Cem (c), $Poly_R$ (e), and Poly (g), average time series for the selected range of particle diameters for samples: Cem_R (b), Cem (d), $Poly_R$ (f), and Poly (h). The data corresponding to the lowest and highest D_p values were excluded due to insufficient data for reliable τ determination, resulting in low statistical significance.

3.2.2 Morphology of worn surfaces for cement-matrix composite

The improved wear resistance of Cem compared to Cem_R can be attributed to its more compact structure, evident in surface micrographs (Figs. 7(a) and 7(c)). The pristine Cem_R surface (Fig. 7(a)) exhibited larger crystallites (ranging from several to tens of micrometres) compared to the more uniform Cem surface (Fig. 7(c)), which showed micrometre- and submicrometre-sized crystallites. Examination of worn surfaces (Figs. 7(b) and 7(d)) revealed extensive

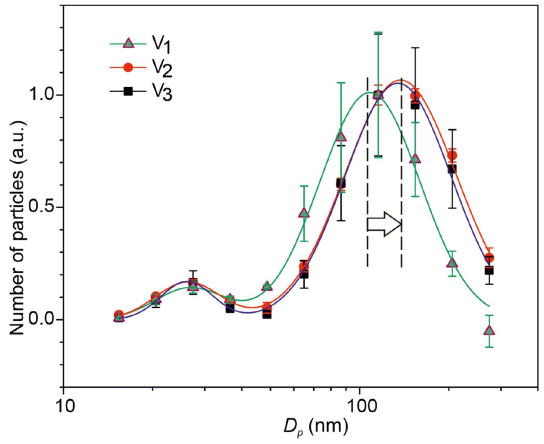

Fig. 5 Normalized distribution functions for aerosols emitted by cementitious samples at times V_1, V_2 and V_3. The dashed lines show the most probable particle size for the dominating mode of the aerosol particle size distributions.

damage to Cem_R, including cracks (red arrows), cutting/ploughing abrasion marks (yellow arrows), and micro-cracking abrasion marks (green arrows). This level of damage is expected, as the hardness of the cement paste is 10 to 20 times lower than that of the alumina pin. In contrast, Cem showed significantly less damage, with only cutting/ploughing abrasion marks (yellow arrow) and micrometer-sized deposits of comminuted crystallites. This observed microstructural difference corroborates the findings of Chen et al. (2020), who reported MWCNT-induced toughening and densification of hydrated ordinary Portland cement, along with a 200% increase in the volume fraction of high-density calcium silicate hydrates and calcium hydroxide. This effect is attributed to the higher surface energy of MWCNTs, which promotes the deposition of hydrated cement products, acting as nucleation sites and ensuring good adhesion (Fakhim et al., 2015).

Detailed observation of the worn Cem surface showed numerous fibrous or rod-like fragments ranging in size from micrometres to submicrometres (Fig. S7). These fragments resemble those observed in the captured aerosols (Fig. 2(c)) and likely must be associated with hydrated phases of Portland cement. Using Energy Dispersive Spectroscopy, we were unable to identify any significant differences in elemental composition between these structures and the surrounding material, which contained elements such as carbon, calcium, silicon, aluminium, and oxygen.

3.2.3 Morphology of worn surfaces for polymer-matrix composite

The addition of MWCNTs significantly influenced the

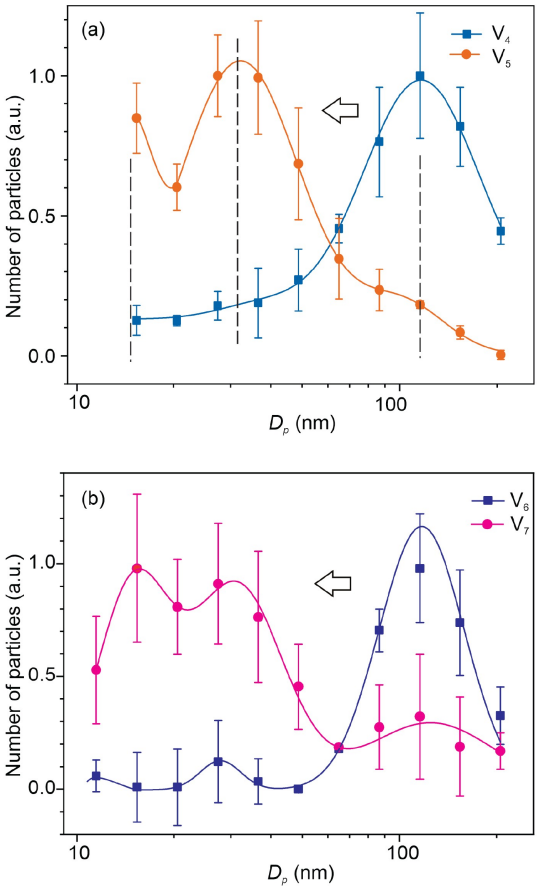

Fig. 6 Normalized distributions of aerosol particles emitted from (a) $Poly_R$ at times V_4, V_5, and (b) Poly at times V_6, V_7.

morphology of the worn polymer composite surface (Fig. 8). The neat polymer surface (Fig. 8(a)) exhibited a high density of surface defects, likely resulting from plastic deformation, fracturing, and debris re-adhesion and merging. Notably, only a few thin abrasion marks were observed. This suggests that adhesive wear was the dominant mechanism.

The composite surface (Fig. 8(b)) also showed signs of plastic deformation. However, it was considerably smoother in comparison with neat polymer and did not exhibit significant structural degradation, likely due to the reinforcing effect of the embedded MWCNTs (Mostovoy et al., 2020). This observation is consistent with previous studies (Düzcükoğlu et al., 2015; Vélez Molina et al., 2025) that reported the formation of a more compact and well-adhered transfer film when MWCNTs were used as additives. Figure 8(c) shows an enlarged view of the wear debris from the polymer composite, revealing two distinct particle types based on aspect ratio. Both types were irregularly shaped and ranged in size from several hundreds of nanometres to

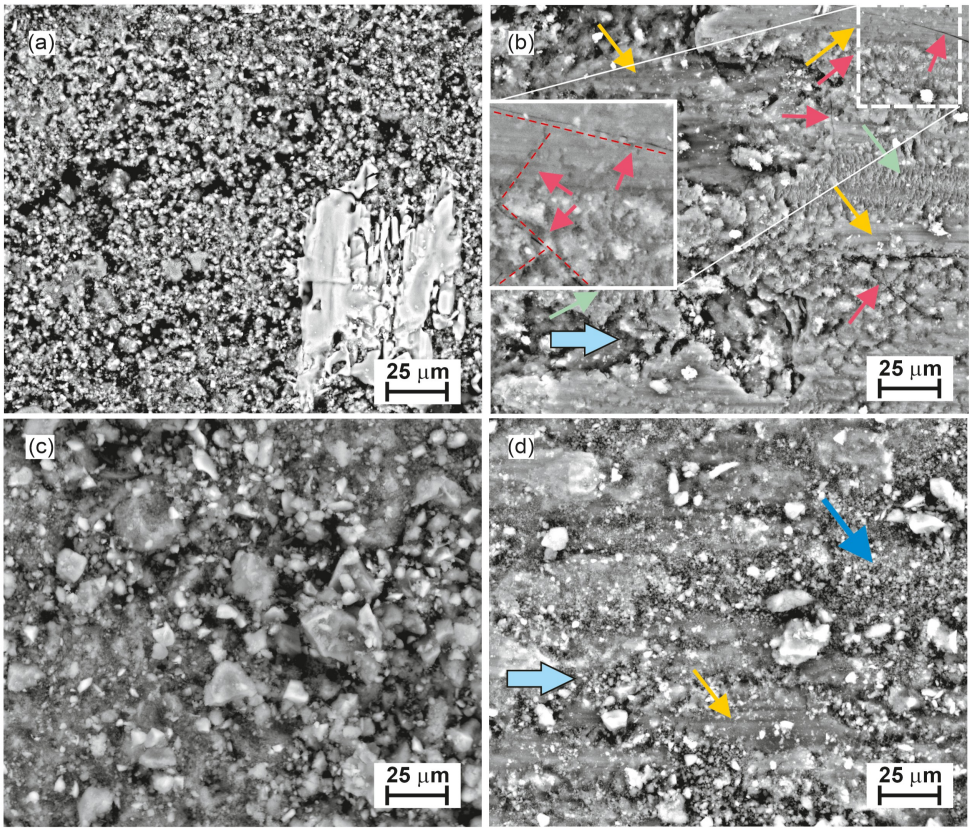

Fig. 7 Micrographs of pristine and worn surfaces of Cem_R and Cem. (a) Pristine Cem_R; (b) worn Cem_R; (c) pristine Cem; (d) worn Cem. Arrows indicate: blue, sliding direction; red, surface cracks; yellow, cutting/ploughing abrasion marks (pristine surfaces); green, micro-cracking abrasion marks and fine debris of cement paste; dark blue, micrometre- and submicrometre-sized comminuted crystallites. Inset in part (b) shows the magnified portion of the image with surface cracks highlighted by red dashed lines.

several micrometres. The high-aspect-ratio particles were likely MWCNT fragments coated with strongly bonded polymer. This suggests that the adhesive bonds between the carbon nanotube surface and the polymer matrix were stronger than the cohesive bonds within the matrix. This finding aligns with the results Eitan et al. (Eitan et al., 2006), who found that polymer chain immobilization due to adsorption on the nanotube surface stiffened the interphase region and provided additional reinforcement to the composite. The results are also consistent with the observation of Guadagno et al. (2009) that the carbon nanotubes are well embedded into the epoxy matrix. This also explains why MWCNT fragments were not liberated from the matrix and not found among the captured aerosol particles.

MWCNTs promoted the formation of a continuous transfer film on the counterpart (Fig. 8(d) and 8(e)) in agreement with previous studies (Campo et al., 2015). This film partially covered the counterpart's contact surface and exhibited weak longitudinal abrasion marks. In contrast, little transfer film formed in the neat polymer experiment; the counterpart surface was significantly rougher, with individual and partially merged wear debris (Fig. 8(d)). The addition of MWCNTs influenced the shape and size of the wear debris. Debris from the neat polymer was irregularly shaped, had a low aspect ratio, and was submicrometer-sized. In contrast, debris from the polymer composite was larger and had a higher aspect ratio. Some of this composite debris (Fig. 8(f)) likely consisted of individual MWCNTs coated with well-adhered polymer. The debris likely originated from abrasion, whereas the rolls were likely formed through a delamination mechanism induced by surface contact, as reported by Zhang (2004). Other, much larger debris particles (Fig. 8(e)) may have formed due to buckling and detachment of elastic waves (Schallamach waves (Viswanathan and Chandrasekar, 2022)) generated on the polymer composite surface by shear forces and the strong adhesive energy between the composite and the counterpart.

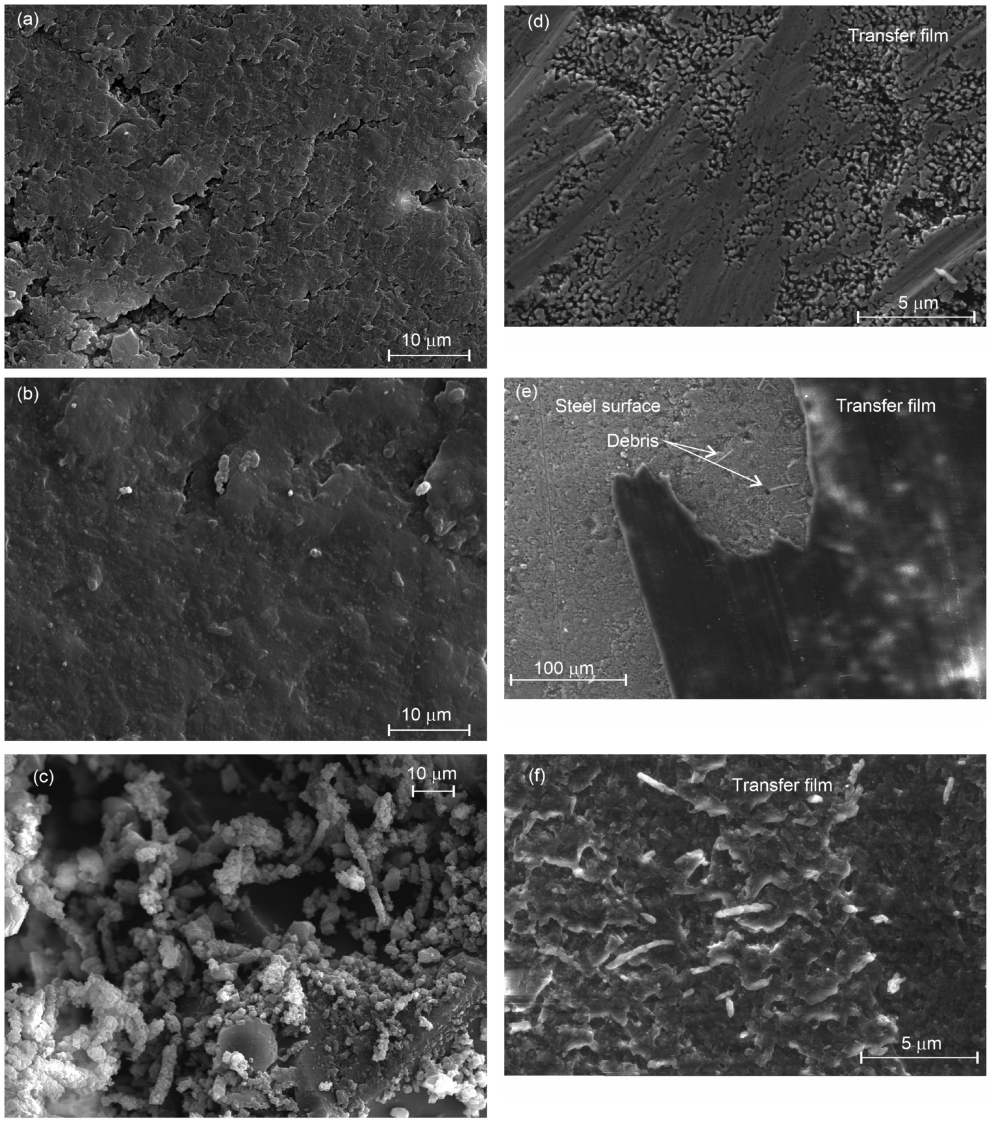

Fig. 8 SEM micrographs of worn surfaces (a) $Poly_R$, (b) Poly; (c) a micrograph of wear debris on Poly worn surface. SEM micrographs of steel disk surface after sliding contact with (d) PolyR, (e) Poly; (f) enlarged view of the transfer film formed due to sliding contact with Poly composite.

3.2.4 Temperature of contact surfaces

Given that the polymer samples remain static during the experiments (Péclet number equals zero), frictional heat generation must be taken into account. The maximum interfacial temperature was estimated by combining the instantaneous ("flash") temperature with the mean temperature rise resulting from heat dissipation at the sliding interface (see Supplementary Information for calculation details and parameters). The calculated maximum temperature rise at the polymer surface by the end of the test was below 50 °C. However, at localized sites of intense plastic deformation and bond rupture—where micrometre- and nanometre-scale debris are formed—the temperature could be higher due to thermomechanical coupling. Previous studies on polyethylene fracture have shown that temperatures at the fracture surface can exceed 70 °C (Guseva et al., 2015; Sorini et al., 2019). Consequently, the temperature of fine and ultrafine debris may transiently reach 140–160 °C or higher. Therefore, partial thermal oxidation of less stable components and free radicals generated by mechanical chain scission cannot be fully ruled out (Capone et al., 2007). Notwithstanding, this temperature is insufficient to cause thermal degradation of bulk vinyl ester (Vélez Molina et al., 2025). In

contrast, for cement composites, both the "flash" temperature and the temperature at fracture sites were significantly lower than for the polymer samples due to the high Péclet number and the brittle nature of the cement paste.

3.3 Structural and tribochemical characterization

3.3.1 Porosity

Although with the addition of MWCNTs the total pore volume nearly doubles, the increase in pore volume occurred mainly for small pores with diameter below 1 μm which may correspond to the voids between individual MWCNTs in the bundles (Shandilya et al., 2015). (Fig. S8, Electronic Supplementary Information which shows the pore volume for Cem_R and Cem as function of pore diameter determined using a mercury intrusion method). In contrast, the volume of larger pores decreased, likely due to the nucleation effect and toughening of cement hydration phases around MWCNTs (Fakhim et al., 2015).

The graph of adsorption isotherm for water (Fig. S1) suggests an open-pore structure. With the addition of MWCNTs the specific surface area determined from water adsorption increased nearly threefold (Table S3). The results suggest a change in the pore structure without significant changing in the surface energy (Thomas et al., 1999).

Similar effect was observed for polymer-matrix composite whose porosity increased nearly twice in comparison with neat polymer (Table 1).

3.3.2 Surface chemical characterization

The Raman spectra of the pristine Cem composite surface (Fig. S9(i)) show bands corresponding to the main hydrated cement phases: calcium silicate hydrate (C–S–H), ettringite, calcium hydroxide, and the products of its carbonation. Two low-intensity broad bands cantered at 1303 cm^{-1} and 1592 cm^{-1} are attributed to sp^2 carbon allotropes (Antunes et al., 2006). After abrasion, the intensity of the bands related to the cement matrix decreased significantly. Notably, the Raman spectrum of the worn surface differed significantly from that of the cross-section (Fig. S9(iii)), indicating that the effect of abrasion cannot be attributed simply to the removal of the topmost surface layer. This suggests a higher degree of disorder in the cement-phase crystallites induced by sliding friction. However, friction did not influence the carbon bands; their positions and intensities remained nearly the same in all three spectra. For reference, spectrum iv (Fig. S9(iv)) was measured on neat MWCNTs. These results are consistent with our microscopic observations, which did not reveal protruding MWCNTs on the pristine Cem surface. They also suggest few, if any, debonded MWCNTs on the abraded surface. Furthermore, no evidence of tribochemical decomposition of MWCNTs, potentially leading to a graphitized surface layer (Cui et al., 2013), was observed on the worn surface. Similar results were obtained for the Poly composite (Fig. S2).

4 Conclusions

The effect of matrix material on the mechanical properties, microstructure, and triboemission of MWCNT-functionalized polymer and cement composites was determined.

MWCNT liberation was not observed in both composites. This suggests that aerosol triboemission was primarily driven by the disintegration of the composite material rather than the release of nanoadditives.

In both matrix systems, MWCNTs influenced the tribological properties and microstructure, notably increasing the volume of submicrometre-sized pores. Previous work showed that incorporation of MWCNTs into a polymer matrix increases storage and elastic moduli likely due to better room-temperature matrix curing promoted by MWCNTs (Vélez Molina et al., 2025). In cement-matrix composites, MWCNTs were reported (Mansouri Sarvandani et al., 2021) to improve compressive strength by filling the cracks, reducing micrometre-size porosity and pore refining. Similar pore refining was observed in this work and associated with higher wear resistance. These changes can have competing effects on wear behaviour and, consequently, on aerosol triboemission. To disentangle the complex relationship between structure, wear rate, and emission rate, the specific emissivity (by volume)—defined as the ratio of emitted aerosol particles to volumetric wear—was calculated for all materials (Table 1).

Interestingly, in the cement-matrix composite, the emissivity increased nearly 15-fold despite a six-fold reduction in wear rate (i.e., increased wear resistance) compared to the reference cement paste. This indicates that although the cement composite generates less total wear debris, the proportion of fine and ultrafine particles within that debris is significantly higher. This increase is attributed to a shift in the scale of matrix disintegration during abrasion—from micrometric to nanometric—likely linked to differences in pore size

distributions between Cem_R and Cem. Emissivity values for Cem_R and Cem closely match those reported for neat cement mortar and polymer-fibre-reinforced cement mortar (Husanu et al., 2024), suggesting that inert components such as sand have minimal influence on aerosol generation mechanisms.

In contrast, no significant change in emissivity was observed between the polymer-matrix composite and its corresponding neat polymer, despite the composite exhibiting reduced surface damage and a greater tendency to form a transfer film. Although the specific wear rate increased slightly, the aerosol emissivity remained stable. MWCNT addition also slightly influenced the aerodynamic characteristics of the emitted particles, narrowing the range of relaxation times across particle sizes without affecting triboemission kinetics.

The divergent effects of MWCNT addition in the two matrix types likely stem from their distinct dominant wear mechanisms: abrasion in the cement composite and adhesion in the polymer composite. This difference likely explains the large disparity in emissivity between cementitious and polymer matrices. While extensive research has focused on debris formation under abrasive wear, the mechanisms of aerosol generation in adhesive wear remain poorly understood. These findings highlight the importance of considering wear mechanisms and composite microstructure when evaluating the environmental and health implications of nanocomposite materials.

Conflicts of Interest The authors declare that the research was conducted in the absence of any commercial or financial relationships that could be construed as a potential conflict of interest.

Acknowledgements This work was supported by Spanish National Research Council (Nos. COOPB20363, COOPA20495, and COOPB24043), Ministry of Science, Innovation and Universities of Spain (Nos. PID2019-111063RB-I00 and TED2021-129950B-I00) and the National Council of Science and Technology of Mexico - CONACYT (No. 740521). The authors acknowledge the FESEM service from the MiNa Laboratory at IMN funded by Madrid's Community Government (No. S2013/ICE2822), Ministry of Science, Innovation and Universities of Spain (No. CSIC13-4E-1794) and EU (FEDER, FSE).

Electronic Supplementary Material Supplementary material is available in the online version of this article at https://dx.doi.org/10.1007/s11783-026-2164-2 and is accessible for authorized users.

Funding Note Open Access funding provided thanks to the CRUE-CSIC agreement with Springer Nature.

References

Antunes E F, Lobo A O, Corat E J, Trava-Airoldi V J, Martin A A, Veríssimo C (2006). Comparative study of first- and second-order Raman spectra of MWCNT at visible and infrared laser excitation. Carbon, 44(11): 2202–2211

Batsungnoen K, Riediker M, Suárez G, Hopf N B (2020). From nano to micrometer size particles – A characterization of airborne cement particles during construction activities. Journal of Hazardous Materials, 398: 122838

Bello D, Wardle B L, Yamamoto N, Guzman Devilloria R, Garcia E J, Hart A J, Ahn K, Ellenbecker M J, Hallock M (2009). Exposure to nanoscale particles and fibers during machining of hybrid advanced composites containing carbon nanotubes. Journal of Nanoparticle Research, 11(1): 231–249

Bello D, Wardle B L, Zhang J, Yamamoto N, Santeufemio C, Hallock M, Virji M A (2010). Characterization of exposures to nanoscale particles and fibers during solid core drilling of hybrid carbon nanotube advanced composites. International Journal of Occupational and Environmental Health, 16(4): 434–450

Boonruksa P, Bello D, Zhang J D, Isaacs J A, Mead J L, Woskie S R (2016). Characterization of potential exposures to nanoparticles and fibers during manufacturing and recycling of carbon nanotube reinforced polypropylene composites. The Annals of Occupational Hygiene, 60(1): 40–55

Borm P J A, Robbins D, Haubold S, Kuhlbusch T, Fissan H, Donaldson K, Schins R, Stone V, Kreyling W, Lademann J, et al. (2006). The potential risks of nanomaterials: a review carried out for ECETOC. Particle and Fibre Toxicology, 3(1): 11

Campo M, Jiménez-Suárez A, Ureña A (2015). Effect of type, percentage and dispersion method of multi-walled carbon nanotubes on tribological properties of epoxy composites. Wear, 324–325: 100–108

Capone C, Di Landro L, Inzoli F, Penco M, Sartore L (2007). Thermal and mechanical degradation during polymer extrusion processing. Polymer Engineering & Science, 47(11): 1813–1819

Cena L G, Peters T M (2011). Characterization and control of airborne particles emitted during production of epoxy/carbon nanotube nanocomposites. Journal of Occupational and Environmental Hygiene, 8(2): 86–92

Cerro-Prada E, Pacheco-Torres R, Varela F (2021). Effect of multi-walled carbon nanotubes on strength and electrical properties of cement mortar. Materials, 14(1): 79

Chen J X, Akono A T (2020). Influence of multi-walled carbon nanotubes on the hydration products of ordinary Portland cement paste. Cement and Concrete Research, 137: 106197

Chen L, Zhu H Y, Cui H H (2017). A study of the Brownian motion of the non-spherical microparticles on fluctuating lattice Boltzmann method. Microfluidics and Nanofluidics, 21(3): 54

Christou A, Stec A A, Ahmed W, Aschberger K, Amenta V (2016). A review of exposure and toxicological aspects of carbon nanotubes, and as additives to fire retardants in polymers. Critical Reviews in Toxicology, 46(1): 74–95

Concha-Lozano N, Muller Y, Favreau P, Suarez G (2025). Determination of ultrafine particle number emission factors from building materials in standardized conditions. Annals of Work Exposures and Health, 69(2): 213–219

Cornelio J A C, Blanco E E, Romero J L, Rudas J S, Guerrero G S, Toro A, Hoyos-Palacio L M (2022). Development of multiwalled carbon nanotubes (MWCNT's) functionalized with molybdenum disulfide (MoS_2) by separate methodology. Diamond and Related Materials, 122: 108814

Cornelio J A C, Cuervo P A, Hoyos-Palacio L M, Lara-Romero J, Toro A (2016). Tribological properties of carbon nanotubes as lubricant additive in oil and water for a wheel–rail system. Journal of Materials Research and Technology, 5(1): 68–76

Cui L J, Geng H Z, Wang W Y, Chen L T, Gao J (2013). Functionalization of multi-wall carbon nanotubes to reduce the coefficient of the friction and improve the wear resistance of multi-wall carbon nanotube/epoxy composites. Carbon, 54: 277–282

Debia M, Bakhiyi B, Ostiguy C, Verbeek J H, Brouwer D H, Murashov V (2016). A systematic review of reported exposure to engineered nanomaterials. The Annals of Occupational Hygiene, 60(8): 916–935

Decarlo P F, Slowik J G, Worsnop D R, Davidovits P, Jimenez J L (2004). Particle morphology and density characterization by combined mobility and aerodynamic diameter measurements. Part 1: theory. Aerosol Science and Technology, 38(12): 1185–1205

Ding Y B, Wohlleben W, Boland M, Vilsmeier K, Riediker M (2017). Nano-object release during machining of polymer-based nanocomposites depends on process factors and the type of nanofiller. Annals of Work Exposures and Health, 61(9): 1132–1144

Duncan T V (2015). Release of engineered nanomaterials from polymer nanocomposites: the effect of matrix degradation. ACS Applied Materials & Interfaces, 7(1): 20–39

Düzcükoğlu H, Ekinci Ş, Şahin Ö S, Avci A, Ekrem M, Ünaldi M (2015). Enhancement of wear and friction characteristics of epoxy resin by multiwalled carbon nanotube and boron nitride nanoparticles. Tribology Transactions, 58(4): 635–642

Eitan A, Fisher F T, Andrews R, Brinson L C, Schadler L S (2006). Reinforcement mechanisms in MWCNT-filled polycarbonate. Composites Science and Technology, 66(9): 1162–1173

Ezzat E N, Al-Saadi I F, Jasim A F (2023). Effect of multiple-walled carbon nanotubes (MWCNTs) on asphalt binder rheological properties and performance. Advances in Civil Engineering, 2023(1): 3248035

Fakhim B, Hassani A, Rashidi A, Ghodousi P (2015). Preparation and microstructural properties study on cement composites reinforced with multi-walled carbon nanotubes. Journal of Composite Materials, 49(1): 85–98

Feijoo I, Pena G, Cabeza M, Cristóbal M J, Rey P (2021). MWCNT-reinforced AA7075 composites: effect of reinforcement percentage on mechanical properties. Metals, 11(6): 969

Golanski L, Gaborieau A, Guiot A, Uzu G, Chatenet J, Tardif F (2011). Characterization of abrasion-induced nanoparticle release from paints into liquids and air. Journal of Physics: Conference Series, 304: 012062

Golanski L, Guiot A, Pras M, Malarde M, Tardif F (2012). Release-ability of nano fillers from different nanomaterials (toward the acceptability of nanoproduct). Journal of Nanoparticle Research, 14(7): 962

Gomez V, Levin M, Saber A T, Irusta S, Dal Maso M, Hanoi R, Santamaria J, Jensen K A, Wallin H, Koponen I K (2014). Comparison of dust release from epoxy and paint nano-composites and conventional products during sanding and sawing. The Annals of Occupational Hygiene, 58(8): 983–994

Guadagno L, Vertuccio L, Sorrentino A, Raimondo M, Naddeo C, Vittoria V, Iannuzzo G, Calvi E, Russo S (2009). Mechanical and barrier properties of epoxy resin filled with multi-walled carbon nanotubes. Carbon, 47(10): 2419–2430

Gupta A, Gaspar D, Yost M, Gross G, Rempes P, Clark M, Martin J (2006). Evaluating the Potential for Release of Carbon Nanotubes and Subsequent Occupational Exposure During Processing of a Nanocomposite. In: Proceedings of Nanotechnology Occupational and Environmental Health and Safety. Washington, DC: ACS Publications, 110–118

Guseva Canu I, Bateson T F, Bouvard V, Debia M, Dion C, Savolainen K, Yu I J (2016). Human exposure to carbon-based fibrous nanomaterials: a review. International Journal of Hygiene and Environmental Health, 219(2): 166–175

Guseva M A, Gerasin V A, Garishin O K, Shadrin V V, Plekhov O A, Pawlak A (2015). Thermal effects under elastic and plastic deformation of polyethylene. Polymer, 56: 416–427

Hammer T, Bossa N, Persson M, Wichser A, Lehner K, Ruggiero E, Fonseca A S, Jovic M, Gaan S, Wohlleben W, et al. (2021). Importance of the number emission factor of combustion-generated aerosols from nano-enabled products. NanoImpact, 22: 100307

Hedmer M, Lovén K, Martinsson J, Messing M E, Gudmundsson A, Pagels J (2022). Real-time emission and exposure measurements of multi-walled carbon nanotubes during production, power sawing, and testing of epoxy-based nanocomposites. Annals of Work Exposures and Health, 66(7): 878–894

Heitbrink W A, Lo L M (2015). Effect of carbon nanotubes upon emissions from cutting and sanding carbon fiber-epoxy composites. Journal of Nanoparticle Research, 17(8): 335

Hennig M P, Maes H M, Ottermanns R, Schäffer A, Siebers N (2019). Release of radiolabeled multi-walled carbon nanotubes (^{14}C-MWCNT) from epoxy nanocomposites into quartz sand-water systems and their uptake by *Lumbriculus variegatus*. NanoImpact, 14: 100159

Hirth S, Cena L, Cox G, Tomović Ž, Peters T, Wohlleben W (2013). Scenarios and methods that induce protruding or released CNTs after degradation of nanocomposite materials. Journal of Nanoparticle Research, 15(4): 1504

Hoyos-Palacio L M, Cuesta Castro D P, Ortiz-Trujillo I C, Botero Palacio L E, Galeano Upegui B J, Escobar Mora N J, Carlos Cornelio J A (2019). Compounds of carbon nanotubes decorated with silver nanoparticles via *in-situ* by chemical vapor deposition (CVD). Journal of Materials Research and Technology, 8(6): 5893–5898

Huang G N, Park J H, Cena L G, Shelton B L, Peters T M (2012). Evaluation of airborne particle emissions from commercial products containing carbon nanotubes. Journal of Nanoparticle Research, 14(11): 1231

Husanu F, Alonso Á, Calderón V, Castellote M, Nevshupa R (2024). Quantitative study of triboemission kinetics from polymer fiber-reinforced mortar paving blocks: unravelling the dynamics of nanoparticle aerosol release. Cement and Concrete Research, 185: 107650

Igartua A, Berriozabal E, Nevshupa R, Roman E, Pagano F, Pleth Nielsen L, Louring S, Muntada L (2017). Screening of diamond-like carbon coatings in search of a prospective solid lubricant suitable for both atmosphere and high vacuum applications. Tribology International, 114: 192–200

Jiang L, Kondo A, Shigeta M, Endoh S, Uejima M, Ogura I, Naito M (2014). Evaluation of particles released from single-wall carbon nanotube/polymer composites with or without thermal aging by an accelerated abrasion test. Journal of Occupational and Environmental Hygiene, 11(10): 658–664

Kang J, Erdely A, Afshari A, Casuccio G, Bunker K, Lersch T, Dahm M M, Farcas D, Cena L (2017). Generation and characterization of aerosols released from sanding composite nanomaterials containing carbon nanotubes. NanoImpact, 5: 41–50

Kasper G (1982). Dynamics and measurement of smokes. I size characterization of nonspherical particles. Aerosol Science and Technology, 1(2): 187–199

Kim J H, Kim W S, Yoo Y (2022). Friction properties of solid lubricants with different multiwalled carbon nanotube contents. Materials, 15(12): 4054

Kim J H, Tugelbayev A, An S H, Lee J U, Chung C W (2024). Dispersion quality of aqueously dispersed MWCNT affected by step sonication process and its impact on mechanical strength of cement paste: a comparison between polycarboxylate based high range water reducers and air entraining agent. Construction and Building Materials, 435: 136712

Koivisto A J, Yu M Z, Hämeri K, Seipenbusch M (2012). Size resolved particle emission rates from an evolving indoor aerosol system. Journal of Aerosol Science, 47: 58–69.

Kovochich M, Fung C C D, Avanasi R, Madl A K (2018). Review of techniques and studies characterizing the release of carbon nanotubes from nanocomposites: implications for exposure and human health risk assessment. Journal of Exposure Science & Environmental Epidemiology, 28(3): 203–215

Kulkarni P, Baron P A, Willeke K (2011). Aerosol Measurement: Principles, Techniques, and Applications. 3rd ed. Hoboken: Wiley, 15–30

Lu X L, Wang S X, Ye Z M, Li C H, Cheng X (2020). Study on the hydration product of ettringite in cement paste with ethanol-diisopropanolamine. Journal of Thermal Analysis and Calorimetry, 139(2): 1007–1016

Makar J M, Chan G W (2009). Growth of cement hydration products on single-walled carbon nanotubes. Journal of the American Ceramic Society, 92(6): 1303–1310

Mansouri Sarvandani M, Mahdikhani M, Aghabarati H, Haghparast Fatmehsari M (2021). Effect of functionalized multi-walled carbon nanotubes on mechanical properties and durability of cement mortars. Journal of Building Engineering, 41: 102407

Methner M, Crawford C, Geraci C (2012). Evaluation of the potential airborne release of carbon nanofibers during the preparation, grinding, and cutting of epoxy-based nanocomposite material. Journal of Occupational and Environmental Hygiene, 9(5): 308–318

Morgeneyer M, Shandilya N, Chen Y M, Le Bihan O (2015). Use of a modified Taber abrasion apparatus for investigating the complete stress state during abrasion and in-process wear particle aerosol generation. Chemical Engineering Research and Design, 93: 251–256

Mostovoy A, Yakovlev A, Tseluikin V, Lopukhova M (2020). Epoxy nanocomposites reinforced with functionalized carbon nanotubes. Polymers, 12(8): 1816

Muñoz-Cortés E, Sánchez-Prieto J, Zabala B, Sanchez C, Flores E, Flores A, Roman E, Ares J R, Nevshupa R (2024). *Operando* exploration of tribochemical decomposition in synthetic FeS_2 thin film and mineral iron pyrite. RSC Mechanochemistry, 1(2): 196–210

Nevshupa R, Castellote M, Cornelio J A C, Toro A (2020). Triboemission of FINE and ultrafine aerosol particles: a new approach for measurement and accurate quantification. Lubricants, 8(2): 21

Nosko O, Borrajo-Pelaez R, Hedström P, Olofsson U (2017). Porosity and shape of airborne wear microparticles generated by sliding contact between a low-metallic friction material and a cast iron. Journal of Aerosol Science, 113: 130–140

Ogura I, Kotake M, Ata S (2019). Quantitative evaluation of carbon nanomaterial releases during electric heating wire cutting and sawing machine cutting of expanded polystyrene-based composites using thermal carbon analysis. Journal of Occupational and Environmental Hygiene, 16(2): 165–178

Ogura I, Kotake M, Shigeta M, Uejima M, Saito K, Hashimoto N, Kishimoto A (2013). Potential release of carbon nanotubes from

their composites during grinding. Journal of Physics: Conference Series, 429: 012049

Ogura I, Okayama C, Kotake M, Ata S, Matsui Y, Gotoh K (2017). Airborne particles released by crushing CNT composites. Journal of Physics: Conference Series, 838: 012015

Ogura I, Shigeta M, Kotake M, Uejima M, Honda K (2015). Particle release from single-wall and multiwall carbon nanotubes in polystyrene-based composites during grinding. Journal of Physics: Conference Series, 617: 012028

Onthong S, Hanpongpun W, Sinthupinyo S, O'Rear E A, Pongprayoon T (2025). Bifunctional multiwall carbon nanotubes and their effect on hydration, conductivity, and mechanical properties of cement composites. International Journal of Concrete Structures and Materials, 19(1): 69

Piscitello A, Bianco C, Casasso A, Sethi R (2021). Non-exhaust traffic emissions: sources, characterization, and mitigation measures. Science of the Total Environment, 766: 144440

Rahman M M, Islam M, Roy R, Younis H, Alnahyan M, Younes H (2022). Carbon nanomaterial-based lubricants: review of recent developments. Lubricants, 10(11): 281

Rasmussen K, Mast J, De Temmerman P J, Verleysen E, Waegeneers N, Van Steen F, Pizzolon J C, De Temmerman L, Van Doren E, Alstrup Jensen K, et al. (2014). Multi-walled carbon nanotubes, NM-400, NM-401, NM-402, NM-403, characterisation and physico-chemical properties. Luxembourg: Publications Office of the European Union, 118

Ren Y, Li F, Cheng H M, Liao K (2003). Tension–tension fatigue behavior of unidirectional single-walled carbon nanotube reinforced epoxy composite. Carbon, 41(11): 2177–2179

Rennhofer H, Zanghellini B (2021). Dispersion state and damage of carbon nanotubes and carbon nanofibers by ultrasonic dispersion: a review. Nanomaterials, 11(6): 1469

R'Mili B, Le Bihan O L C, Dutouquet C, Aguerre-Charriol O, Frejafon E (2013). Particle sampling by TEM grid filtration. Aerosol Science and Technology, 47(7): 767–775

Rusanov A, Nevshupa R, Fontaine J, Martin J M, Le Mogne T, Elinson V, Lyamin A, Roman E (2015a). Probing the tribo-chemical degradation of hydrogenated amorphous carbon using mechanically stimulated gas emission spectroscopy. Carbon, 81: 788–799

Rusanov A, Nevshupa R, Martin J M, Garrido M Á, Roman E (2015b). Tribochemistry of hydrogenated amorphous carbon through analysis of Mechanically Stimulated Gas Emission. Diamond and Related Materials, 55: 32–40

Saber A T, Mortensen A, Szarek J, Koponen I K, Levin M, Jacobsen N R, Pozzebon M E, Mucelli S P, Rickerby D G, Kling K, et al. (2015). Epoxy composite dusts with and without carbon nanotubes cause similar pulmonary responses, but differences in liver histology in mice following pulmonary deposition. Particle and Fibre Toxicology, 13(1): 37

Scheuch G, Heyder J (1990). Dynamic shape factor of nonspherical aerosol particles in the diffusion regime. Aerosol Science and Technology, 12(2): 270–277

Schlagenhauf L, Chu B T T, Buha J, Nüesch F, Wang J (2012). Release of carbon nanotubes from an epoxy-based nano-composite during an abrasion process. Environmental Science & Technology, 46(13): 7366–7372

Schlagenhauf L, Kuo Y Y, Michel S, Terrasi G, Wang J (2015). Exposure assessment of a high-energy tensile test with large carbon fiber reinforced polymer cables. Journal of Occupational and Environmental Hygiene, 12(8): D178–D183

Schraufnagel D E (2020). The health effects of ultrafine particles. Experimental & Molecular Medicine, 52(3): 311–317

Sedaghatdoost A, Behfarnia K (2018). Mechanical properties of Portland cement mortar containing multi-walled carbon nanotubes at elevated temperatures. Construction and Building Materials, 176: 482–489

Shandilya N, Le Bihan O, Morgeneyer M (2014). A review on the study of the generation of (nano)particles aerosols during the mechanical solicitation of materials. Journal of Nanomaterials, 2014(1): 289108

Shandilya N, Morgeneyer M, Le Bihan O (2015). First development to model aerosol emission from solid surfaces subjected to mechanical stresses: I. Development and results. Journal of Aerosol Science, 89: 43–57

Sharma M, Shatkin J A, Cairns C, Canady R, Clippinger A J (2016). Framework to evaluate exposure relevance and data needs for risk assessment of nanomaterials using *in vitro* testing strategies. Risk Analysis, 36(8): 1551–1563

Shirasu K, Miyaura T, Yamamoto G, Suzuki T, Naito K, Hashida T (2020). Enhanced tribological performance of alumina composites reinforced with acid-treated carbon nanotubes under water lubrication. Diamond and Related Materials, 101: 107657

Sorini C, Chattopadhyay A, Goldberg R K (2019). Micromechanical modeling of the effects of adiabatic heating on the high strain rate deformation of polymer matrix composites. Composite Structures, 215: 377–384

Starost K, Frijns E, Van Laer J, Faisal N, Egizabal A, Elizextea C, Blazquez M, Nelissen I, Njuguna J (2017). Assessment of nanoparticles release into the environment during drilling of carbon nanotubes/epoxy and carbon nanofibres/epoxy nano-composites. Journal of Hazardous Materials, 340: 57–66

Thomas J J, Jennings H M, Allen A J (1999). The surface area of hardened cement paste as measured by various techniques. Concrete Science and Engineering, 1: 45–64

Thompson D, Chen S C, Wang J, Pui D Y H (2015). Aerosol emission monitoring and assessment of potential exposure to multi-walled carbon nanotubes in the manufacture of polymer nanocomposites. The Annals of Occupational Hygiene, 59(9): 1135–1151

Vélez J C, Cornelio J A C, Sierra R B, Santa J F, Hoyos-Palacio L M, Nevshupa R, Toro A (2020). Development of a composite friction modifier with carbon nanotubes for applications at the wheel–rail interface. Advanced Composites Letters, 29: 2633366X20930019

Vélez Molina J C, Carlos Cornelio J A, Buitrago-Sierra R, Santa

Marin J F, Hoyos-Palacio L M, Cacua K, Rudas J S, Toro A, Nevshupa R (2025). Exploring synergistic and antagonistic interactions of MoS_2 and multi-wall carbon nanotube additives in a composite top-of-rail friction modifier. Tribology International, 207: 110611

Viswanathan K, Chandrasekar S (2022). Fifty years of Schallamach waves: from rubber friction to nanoscale fracture. Philosophical Transactions of the Royal Society A: Mathematical, Physical and Engineering Sciences, 380(2232): 20210339

Wahlström J, Olander L, Olofsson U (2010). Size, shape, and elemental composition of airborne wear particles from disc brake materials. Tribology Letters, 38(1): 15–24

Wohlleben W, Bossa N, Mitrano D M, Scott K (2024). Everything falls apart: How solids degrade and release nanomaterials, composite fragments, and microplastics. NanoImpact, 34: 100510

Wohlleben W, Brill S, Meier M W, Mertler M, Cox G, Hirth S, Von Vacano B, Strauss V, Treumann S, Wiench K, et al. (2011). On the lifecycle of nanocomposites: comparing released fragments and their *in-vivo* hazards from three release mechanisms and four nanocomposites. Small, 7(16): 2384–2395

Wohlleben W, Meier M W, Vogel S, Landsiedel R, Cox G, Hirth S, Tomović Ž (2013). Elastic CNT–polyurethane nanocomposite: synthesis, performance and assessment of fragments released during use. Nanoscale, 5(1): 369–380

Wu Y H, Dong C L, Yuan C Q, Bai X Q, Zhang L Y, Tian Y (2021). MWCNTs filled high-density polyethylene composites to improve tribological performance. Wear, 477: 203776

Xie H M, Wei Y Y, Jiang B, Tang C P, Nie C Y (2021). Tribological properties of carbon nanotube/SiO_2 combinations as water-based lubricant additives for magnesium alloy. Journal of Materials Research and Technology, 12: 138–149

Ye X Y, E S F, Fan M J (2019). The influences of functionalized carbon nanotubes as lubricating additives: length and diameter. Diamond and Related Materials, 100: 107548

Zhang L C, Zarudi I, Xiao K Q (2006). Novel behaviour of friction and wear of epoxy composites reinforced by carbon nanotubes. Wear, 261(7−8): 806–811

Zhang L G, Zhang G, Chang L, Wetzel B, Jim B, Wang Q H (2016). Distinct tribological mechanisms of silica nanoparticles in epoxy composites reinforced with carbon nanotubes, carbon fibers and glass fibers. Tribology International, 104: 225–236

Zhang S W (2004). Tribology of Elastomers. Amsterdam: Elsevier

Zhang X F, Luster B, Church A, Muratore C, Voevodin A A, Kohli P, Aouadi S, Talapatra S (2009). Carbon nanotube−MoS_2 composites as solid lubricants. ACS Applied Materials & Interfaces, 1(3): 735–739

Zhao Y, Goodwin D G, Sung L, Ramakrishnan G, Wu Q Y, Cen J J, Petersen E J, Orlov A (2023). Quantitative evaluation of released nanomaterials from carbon nanotube epoxy nanocomposites during environmental exposure and mechanical treatment. NanoImpact, 32: 100486